European Journal of Medicinal Chemistry 257 (2023) 115419

Contents lists available at ScienceDirect

European Journal of Medicinal Chemistry

journal homepage: www.elsevier.com/locate/ejmech

Research paper

Structure-based virtual screening discovers potent and selective adenosine A_1 receptor antagonists

Pierre Matricon [a,1], Anh TN. Nguyen [b,1], Duc Duy Vo [a,1], Jo-Anne Baltos [b,1], Mariama Jaiteh [a], Andreas Luttens [a], Stefanie Kampen [a], Arthur Christopoulos [b], Jan Kihlberg [c], Lauren Therese May [b,**], Jens Carlsson [a,*]

[a] *Science for Life Laboratory, Department of Cell and Molecular Biology, Uppsala University, SE-751 24, Uppsala, Sweden*
[b] *Drug Discovery Biology, Monash Institute of Pharmaceutical Sciences, Monash University, Parkville, Victoria, 3052, Australia*
[c] *Department of Chemistry - BMC, Uppsala University, SE-751 23, Uppsala, Sweden*

ARTICLE INFO

Keywords:
Molecular docking
Computer-aided drug design
G protein-coupled receptor
Selectivity

ABSTRACT

Development of subtype-selective leads is essential in drug discovery campaigns targeting G protein-coupled receptors (GPCRs). Herein, a structure-based virtual screening approach to rationally design subtype-selective ligands was applied to the A_1 and A_{2A} adenosine receptors (A_1R and $A_{2A}R$). Crystal structures of these closely related subtypes revealed a non-conserved subpocket in the binding sites that could be exploited to identify A_1R selective ligands. A library of 4.6 million compounds was screened computationally against both receptors using molecular docking and 20 A_1R selective ligands were predicted. Of these, seven antagonized the A_1R with micromolar activities and several compounds displayed slight selectivity for this subtype. Twenty-seven analogs of two discovered scaffolds were designed, resulting in antagonists with nanomolar potency and up to 76-fold A_1R-selectivity. Our results show the potential of structure-based virtual screening to guide discovery and optimization of subtype-selective ligands, which could facilitate the development of safer drugs.

1. Introduction

G protein-coupled receptors (GPCRs) constitute the largest group of eukaryotic cell surface proteins, which are activated by extracellular stimuli and trigger intracellular signaling pathways. More than 800 GPCRs are encoded in the human genome and 34% of currently approved drugs mediate their effect by interacting with members of this superfamily [1]. Over the last decade, the determination of atomic resolution structures by X-ray crystallography and electron cryo-microscopy have revealed the binding sites of numerous GPCRs, which is anticipated to accelerate the development of novel drugs [2]. In early drug discovery, a primary goal is to identify high-affinity ligands of the target GPCR with the desired functional effect. It is also essential that the compounds bind selectively to avoid side effects due to off-target interactions, which remain a common cause of adverse effects of approved drugs and failures in clinical trials [3,4]. However, as many GPCRs recognize the same or similar ligands, achieving target selectivity may be challenging. There is generally a strong sequence conservation in the binding site among receptor subtypes that recognize the same endogenous ligand. Access to atomic resolution GPCR structures provides the opportunity to identify differences between closely related targets and guide rational design of selective ligands [5].

Adenosine receptors are a family of GPCRs that comprise four subtypes (A_1, A_{2A}, A_{2B}, and A_3). Activation of the A_1R and A_3R leads to signaling through $G_{i/o}$ proteins that decrease adenylate cyclase activity and as a result intracellular cAMP, whereas the $A_{2A}R$ and $A_{2B}R$ activate G_s proteins, which stimulate cAMP production [6]. Moreover, adenosine receptors can modulate a range of intracellular signaling pathways, in addition to cAMP, such as ERK1/2 phosphorylation and calcium mobilization [7–11]. Adenosine receptors are widely expressed in human

---

Abbreviations: A_1R, adenosine A_1 receptor; $A_{2A}R$, adenosine A_{2A} receptor; $A_{2B}R$, adenosine A_{2B} receptor; A_3R, adenosine A_3 receptor; GPCR, G protein-coupled receptor; NECA, 5′-N-ethylcarboxamidoadenosine; PAINS, Pan-assay interference compounds.

* Corresponding author.

** Corresponding author.

E-mail addresses: lauren.may@monash.edu (L.T. May), jens.carlsson@icm.uu.se (J. Carlsson).

[1] These authors contributed equally.

https://doi.org/10.1016/j.ejmech.2023.115419
Received 12 January 2023; Received in revised form 24 April 2023; Accepted 25 April 2023
Available online 1 May 2023
0223-5234/© 2023 The Authors. Published by Elsevier Masson SAS. This is an open access article under the CC BY license (http://creativecommons.org/licenses/by/4.0/).

tissues and have been identified as therapeutic targets in several conditions [12]. The first crystal structure of an adenosine receptor, the $A_{2A}R$ subtype, was determined in 2008 [13]. Virtual screens of chemical libraries and lead optimization efforts demonstrated that the $A_{2A}R$ was an excellent target for a structure-based approach, leading to the design of a large number of high-affinity ligands [14–17]. Notably, these efforts resulted in the first example of a clinical candidate developed with the use of structure-based drug design, the antagonist HTL-1071 (ADZ4635), which is currently being evaluated as an anti-cancer drug [18]. However, the development of adenosine receptor therapeutics has also been hampered by adverse effects. The $A_{2A}R$ antagonist tozadenant was terminated in phase III trials due to the deaths of several patients, which were likely caused by off-target interactions [19].

To date, rational development of selective GPCR ligands has been limited by a paucity of high resolution receptor structures, in particular across receptor subtypes. However, recent advances enabling a rapid pace of GPCR structure determination will make it possible to consider panels of targets and anti-targets in structure-based ligand design [20]. In the case of adenosine receptors, subtype-selective compounds are essential in drug development due to the broad distribution and varied roles of the subtypes [12]. Comparison of the recently determined structures of the A_1R with the $A_{2A}R$ provided the first insights into structural variation between these closely related receptor subtypes [21, 22]. The A_1/A_{2A} receptor pair hence represents a prototypical example of the challenges involved in designing GPCR drugs and can contribute to the development of more efficient strategies to identify selective probes.

In this study, we explored the use of GPCR structures of multiple subtypes to discover selective ligands by virtual screening of chemical libraries. The A_1/A_{2A} receptor pair was selected with the goal of identifying antagonists with high A_1R affinity and subtype selectivity over the $A_{2A}R$. Such ligands would provide starting points for the development of drugs to treat renal dysfunction associated with chronic heart disease [23]. Molecular docking programs have been demonstrated to perform well for GPCRs with enclosed binding pockets (e.g., the adenosine, histamine, and dopamine receptors) [20]. Several successful structure-based virtual screens have been carried out for such targets, and detailed protocols for docking screens of large commercially available libraries were recently described [24]. Here, molecular docking was used to screen a library of 4.6 million compounds against A_1R and $A_{2A}R$ crystal structures with the goal to identify selective ligands. A set of compounds that were predicted to bind selectively to the A_1R were evaluated in biological assays. The design of chemical libraries guided by the receptor structures enabled rapid optimization of two virtual screening hits to nanomolar antagonists displaying A_1R selectivity.

2. Results

2.1. Molecular docking screens for A_1R selective antagonists

Crystal structures of the A_1R and $A_{2A}R$ were analyzed to identify differences in the binding sites that could be exploited to discover subtype-selective ligands. Whereas only one crystal structure of the A_1R subtype had been determined at the start of this work, a large number of $A_{2A}R$ structures in complex with diverse ligands were available [25]. The structures revealed that the binding sites of these adenosine receptors are very similar. Of the 13 residues forming the ligand binding site in the structure of the A_1R-DU172 complex, 11 are identical to the residues in the $A_{2A}R$. Only Leu253$^{6\times54}$ and Thr270$^{7\times34}$ (generic residue numbers in superscript [26]) in the A_1R, which are located in the extracellular entrance to the binding site, were replaced by other residues in the $A_{2A}R$ pocket (Ile252$^{6\times54}$ and Met270$^{7\times34}$, respectively). The two less bulky side chains in the A_1R created a unique subpocket that provided a structural interpretation of the selectivity of DU172, which positions a bulky cyclohexane group in this region [22]. The same binding mode in the $A_{2A}R$ structure would lead to a steric clash with Met270$^{7\times34}$ (Fig. 1). The ensemble of determined $A_{2A}R$ structures showed that the orthosteric site could adopt different shapes that varied in similarity to the A_1R. For example, Glu169^{ECL2} (Glu172^{ECL2} in A_1R) and His264^{ECL3} form a salt bridge in the opening of the $A_{2A}R$ orthosteric site in several crystal structures. However, there is also an alternative rotamer of Glu169^{ECL2}, leading to a subpocket that resembles that observed in the A_1R structure to a larger extent. The region that appeared responsible for the selectivity of DU172 hence displayed a high degree of plasticity in the $A_{2A}R$. The high sequence conservation and binding site flexibility of these adenosine receptors illustrate the complexity of designing subtype-selective GPCR ligands.

To identify selective A_1R antagonists, we used structure-based virtual screening of a chemical library containing 4.6 million commercially available compounds (Fig. 2). Each compound in the library was first docked to the orthosteric site of the A_1R using the program DOCK3.6 and a binding energy was predicted using a physics-based scoring function [27]. As available $A_{2A}R$ structures showed that this receptor could adopt a spectrum of binding site conformations, an ensemble representing six shapes were used in the virtual screen. The same chemical library was docked to the $A_{2A}R$ binding sites and the compounds were ranked by score to each structure. In total, the structures of >32 million complexes were predicted in the docking screen and, in each case, thousands of ligand poses were typically explored.

The top 6000 compounds from the A_1R screen, corresponding to 0.1% of the library, were further filtered based on their best score from the six $A_{2A}R$ screens. As comparison of energy scores for the two receptor subtypes could be misleading due to limitations of the docking method (e.g., neglect of receptor conformational energy), we used the difference in rank of each compound to predict selectivity. The 700 compounds with the largest differences in rank between the A_1R and $A_{2A}R$ screens were selected for further evaluation. The difference in docking rank for these compounds ranged from 134927 to 2728013. This set of compounds was hence top-scored for the A_1R, but had substantially lower ranking in all the $A_{2A}R$ screens. The interactions of these compounds in the A_1R binding site were analyzed in more detail. Encouragingly, consideration of the set of $A_{2A}R$ screens led to an enrichment of compounds occupying pockets that were unique for the A_1R. For example, 74% of the compounds positioned substituents in the vicinity of Thr270$^{7\times34}$ in the A_1R site and would hence clash with Met270$^{7\times34}$ in the $A_{2A}R$. For comparison, only 55% occupied this region among the top-ranked compounds from the A_1R screen alone. Finally, 20 diverse compounds (**1**-**20**) that formed hydrogen bonds with Asn254$^{6\times55}$ and interacted with non-conserved regions in the A_1R structure were selected for experimental evaluation (Table 1 and Table S1).

2.2. Pharmacological evaluation of predicted ligands

The pharmacology of the 20 compounds selected from the virtual screening was assessed at the human A_1R and $A_{2A}R$ based on a canonical G protein signaling pathway, modulation of cAMP accumulation. A_1R activation of $G_{i/o}$ proteins decreases forskolin-stimulated cAMP accumulation, whereas $A_{2A}R$ activation of G_s proteins stimulates cAMP accumulation. The influence of the selected 20 compounds on the potency of an adenosine receptor agonist (NECA) was quantified in FlpInCHO cells stably expressing the human A_1R (A_1R-FlpInCHO) or human $A_{2A}R$ ($A_{2A}R$-FlpInCHO). In the absence of NECA, compounds (10 μM) did not cause a significant change in baseline cAMP accumulation in either A_1R-FlpInCHO or $A_{2A}R$-FlpInCHO cells, demonstrating that they are not agonists. Seven compounds significantly decreased the NECA potency at the A_1R ($P < 0.05$; one-way ANOVA, Dunnett's post-hoc test), corresponding to an on-target screening hit rate of 35% (Fig. 3A, Fig. S1, and Table 1). At the $A_{2A}R$, nine compounds significantly decreased NECA potency ($P < 0.05$; one-way ANOVA, Dunnett's post-hoc test) (Fig. 3A, Fig. S1, and Table 1). Although the screening hit rates for the target (A_1R) and anti-target ($A_{2A}R$) were similar, among the most active

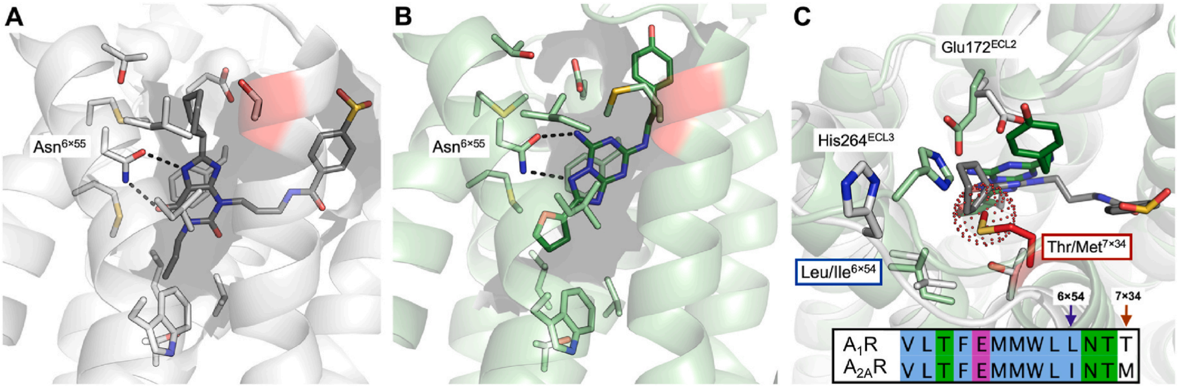

Fig. 1. Comparison of the orthosteric binding sites of the A_1R and $A_{2A}R$. (A) Crystal structure of the A_1R in complex with DU172 (PDB code: 5UEN). (B) Crystal structure of the $A_{2A}R$ in complex with ZM241385 (PDB code: 4EIY). (C) Comparison of the extracellular region of the A_1R and $A_{2A}R$ binding sites. Of the 13 binding sites residues shown in the sequence alignment, all are identical except Thr270$^{7\times34}$ and Leu253$^{6\times54}$ (A_1R), which are methionine and isoleucine in the $A_{2A}R$, respectively. Based on alignment of the A_1R and $A_{2A}R$ structures, Met270$^{7\times34}$ would clash with DU172. The clash is illustrated by showing the Cε atom of Met270$^{7\times34}$ as a red-dotted sphere. The receptors are shown as cartoons (A_1R and $A_{2A}R$ in white and green, respectively). The region corresponding to the Thr/Met$^{7\times34}$ selectivity hot spot is colored in red. Ligands and selected side chains are shown as sticks. Receptor-ligand hydrogen bonds are shown as black dashed lines.

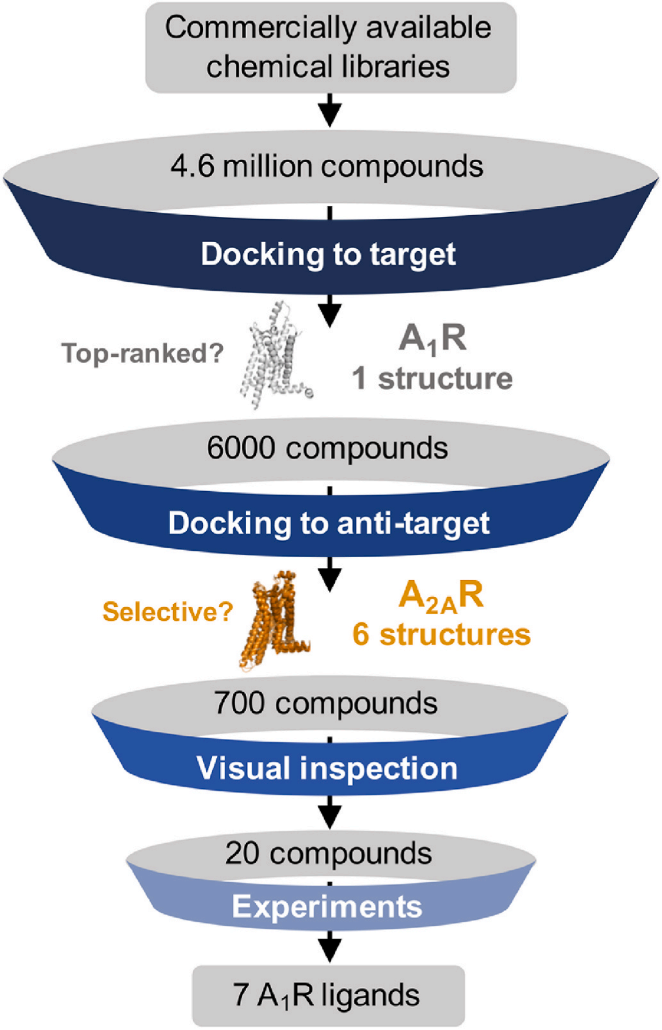

Fig. 2. Workflow of the structure-based virtual screen for A_1R ligands.

compounds, there was a trend toward a greater effect, and as such higher affinity at the A_1R. Five compounds caused a ~10-fold decrease in NECA potency at the A_1R, whereas only three led to a similar shift at the $A_{2A}R$. Compound **8** caused the greatest inhibition at both the A_1R and $A_{2A}R$, decreasing NECA potency approximately 60- and 15-fold, respectively. The seven compounds that significantly decreased NECA potency at the A_1R were further characterized in [^{3}H]DPCPX radioligand binding using A_1R-FlpInCHO cells. The affinity (pK_I) of compounds determined from radioligand binding ranged from 0.2 to 3 μM (Table 1). In accordance with functional studies, compound **8** had the highest A_1R affinity.

The discovered ligands represented diverse scaffolds, but were all predicted to be buried deep within the transmembrane orthosteric site and have similar interactions with the receptor. All compounds formed hydrogen bonds with Asn254$^{6\times55}$ and extended into the subpocket formed by Thr270$^{7\times34}$ with aliphatic or aromatic moieties (Fig. 4). Compound novelty was evaluated by calculating the 2D similarity to known A_1R and $A_{2A}R$ antagonists from the ChEMBL [28–30] and IUPHAR/BPS Guide to Pharmacology [31] databases. The Tanimoto similarity coefficients (T_c) ranged from 0.27 to 0.45 (Table 1 and Table S2). Several compounds displayed overall low similarity to the closest known antagonists ($T_c \leq = 0.30$: compounds **2**, **5** and **10**) (Table S2). Compounds **19** and **20** were more similar to known ligands ($T_c = 0.43$–0.45) and based on previously identified xanthine and 2-aminopyrimidine cores [32]. The 2-aminothiazole-based compound **8** ($T_c = 0.36$) was later identified to be similar to A_1R ligands described by Göblyös et al. ($T_c = 0.65$), which were not present in the ChEMBL or IUPHAR/BPS Guide to Pharmacology databases (Table 1 and Table S2) [33].

2.3. Structure-guided ligand optimization

Based on the pharmacology alongside scaffold diversity and synthetic feasibility of analogs, compounds **8** and **19** were taken forward for detailed functional interactions. NECA concentration-response curves in the absence or presence of increasing concentrations (0.3–30 μM) of **8** or **19** were performed (Fig. 3B and 3C). Both compounds caused a concentration-dependent decrease in NECA potency, with global analysis of functional interactions preferentially fitting to a model of competitive antagonism, supporting the predicted binding modes. Compounds **8** (Table 2) and **19** (Table 3) had estimated affinities (K_B) in the low micromolar range, approximately 0.9 μM and 2.7 μM, respectively. These two scaffolds were further optimized for A_1R affinity and subtype selectivity. In the hit optimization step, tailored chemical libraries with analogs of the two hits were generated and docked into both the A_1R and $A_{2A}R$ crystal structures, followed by synthesis and biological evaluation of promising candidates.

Analysis of the predicted binding mode of compound **8** suggested that this ligand was anchored deeply in the orthosteric site and achieved

Table 1
Experimental evaluation of predicted ligands from the virtual screen (**1**-**20**).

ID	Rank[a]	ΔRank[b]	2D structure[c]	pK_I[d]	pEC_{50}[e]		T_c[f]
	A_1R	$A_{2A}R$		A_1R	A_1R	$A_{2A}R$	
NECA	N/A[g]	N/A	–		8.74 ± 0.08	8.38 ± 0.03	N/A
DPCPX	N/A	N/A	–	9.08 ± 0.11			N/A
1	–	–	–		8.68 ± 0.13	8.34 ± 0.05	–
2	711	208,506	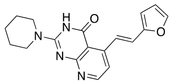	5.58 ± 0.12	7.98 ± 0.07*	8.17 ± 0.05	0.27
3	–	–	–	–	8.55 ± 0.13	7.98 ± 0.03*	–
4	–	–	–	–	8.60 ± 0.17	7.93 ± 0.05*	–
5	5179	622,570	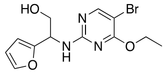	5.61 ± 0.14	7.83 ± 0.28*	7.67 ± 0.05*	0.30
6	–	–	–	–	8.72 ± 0.20	8.36 ± 0.04	–
7	–	–	–	–	8.79 ± 0.17	8.35 ± 0.05	–
8	2944	162,244	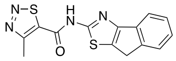	6.67 ± 0.07	6.93 ± 0.13*	7.20 ± 0.09*	0.36/0.65[h]
9	–	–	–	–	8.59 ± 0.28	7.69 ± 0.05*	–
10	1477	564,866	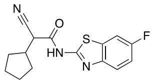	6.29 ± 0.09	7.42 ± 0.25*	7.32 ± 0.10*	0.29
11	–	–	–	–	8.59 ± 0.15	8.27 ± 0.07	–
12	–	–	–	–	8.44 ± 0.16	8.22 ± 0.08	–
13	–	–	–	–	8.49 ± 0.10	7.73 ± 0.07*	–
14	3796	250,964	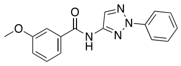	6.00 ± 0.10	7.67 ± 0.11*	7.23 ± 0.13*	0.38
15	–	–	–	–	8.48 ± 0.19	8.34 ± 0.09	–
16	–	–	–	–	8.60 ± 0.26	8.34 ± 0.06	–
17	–	–	–	–	8.60 ± 0.11	8.34 ± 0.05	–
18	–	–	–	–	8.63 ± 0.12	8.34 ± 0.08	–
19	3829	289,227	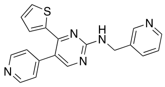	5.81 ± 0.07	7.60 ± 0.10*	7.91 ± 0.08*	0.43
20	2898	969,415	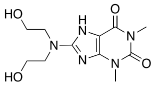	5.55 ± 0.05	7.77 ± 0.11*	8.16 ± 0.06	0.45

*$p < 0.05$, one-way analysis of variance with Dunnett's post-test significant relative to NECA alone.

[a] Docking rank of selected compounds from the A_1R screen of 4.6 million compounds.

[b] The smallest difference in rank between the A_1R and the six $A_{2A}R$ docking screens.

[c] Structures and data from the virtual screen for compounds that were inactive at the A_1R are shown in Table S1.

[d] Compound affinity (pK_I) determined from radioligand binding assays. Values represent the mean ± SEM from n = 3 individual replicates performed in duplicate.

[e] NECA potency (pEC_{50}) determined from cAMP accumulation assays in the absence or presence of 10 μM compound in A_1R-FlpInCHO or $A_{2A}R$-FlpInCHO cells. Values represent the mean ± SEM from n = 3–4 independent experiments performed in duplicate.

[f] Tanimoto coefficient for the most similar orthosteric A_1R or $A_{2A}R$ ligand reported in the ChEMBL and IUPHAR/BPS Guide to Pharmacology databases. Structures of the most similar ligands are shown in Table S2.

[g] N/A denotes not applicable.

[h] Compound **8** ($T_c = 0.36$) was later identified to be more similar to a series of A_1R ligands that were not present in the ChEMBL or IUPHAR/BPS Guide to Pharmacology databases ($T_c = 0.65$).

selectivity by extending into the non-conserved pocket in the extracellular entrance of the binding site. However, the 1,2,3-thiadiazole moiety was small and polar, which did not complement the hydrophobic nature of the pocket optimally. In order to identify alternative substituents that could extend into the same pocket, searches for analogs in libraries of commercially available compounds were performed, and a virtual library containing synthetically accessible analogs was designed. The virtual library was created by identifying commercially available building blocks compatible with amide coupling (Fig. 5A), followed by *in silico* generation of analogs in which the thiadiazole moiety of compound **8** was replaced by diverse chemical groups. A set of 2735 compounds was docked to the orthosteric site of the A_1R and inspected visually. Of these, 19 top-ranked compounds were selected based on an overall conserved binding mode and positioning of bulkier substituents in the non-conserved pocket. Both aliphatic and aromatic substituents were explored and all of these were predicted to fit better in the A_1R binding site. Nine compounds were custom synthesized by a commercial vendor (**22a-i**), and 10 compounds were prepared by amide coupling of **21** with acyl chloride derivatives (**22j-m**) or with carboxylic acid derivatives using HATU as coupling reagent (**22n-s**, Fig. 5A). The functional affinity (pK_B) of compound **8** derivatives at the A_1R and $A_{2A}R$ were determined from functional inhibition cAMP assays, interacting an EC_{80} concentration of agonist against increasing compound concentrations (1 nM–30 μM), with compound affinity values derived using Equations (3)–(5). A first series of aromatic substituents (compounds **22a-g**) did not significantly increase affinity at the A_1R (Fig. 5B, Table 2, and Fig. S2). In contrast, aliphatic substituents could improve potency and selectivity. Of the 12 compounds in this series (**22h-s**), eight had significantly greater affinity and, of these, compounds **22h** and **22l** had significantly greater selectivity for the A_1R compared to the $A_{2A}R$ (Fig. 5B and Fig. S2). In particular, compound **22l** had nanomolar affinity (estimated K_B of 27 nM) and ~20-fold higher affinity for the A_1R

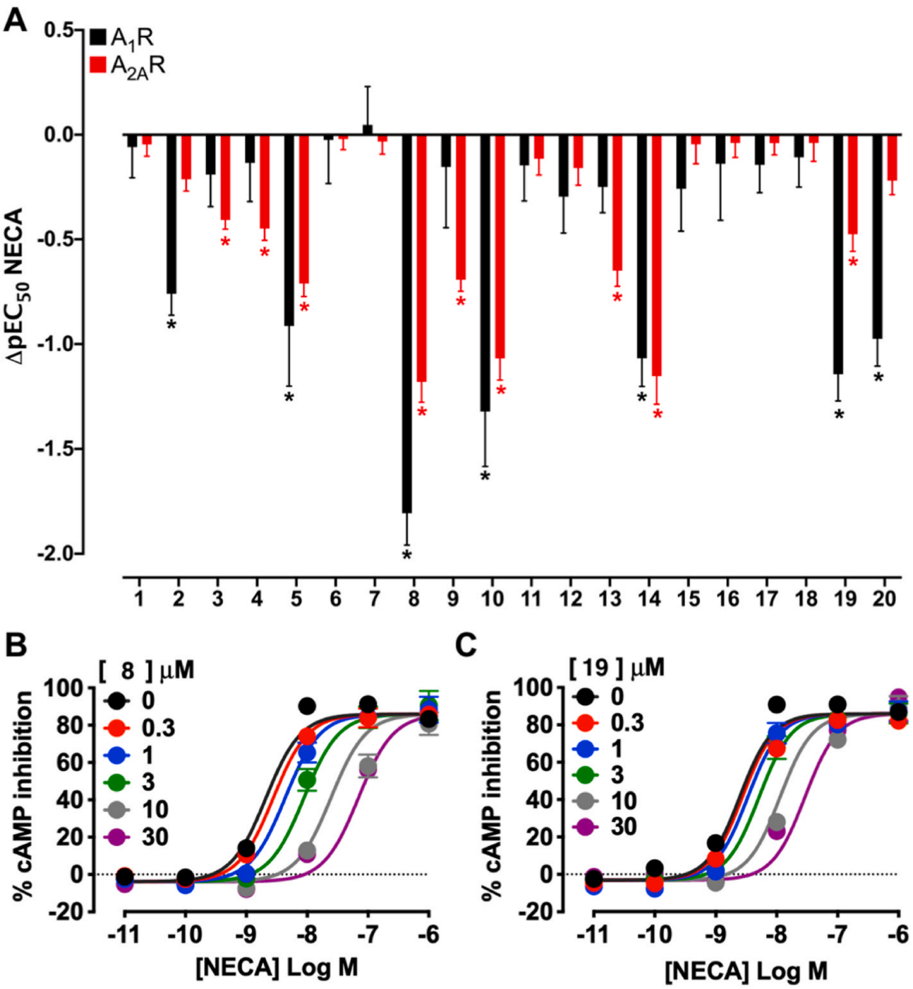

Fig. 3. Pharmacological assessment of virtual screening hits at the A_1R and $A_{2A}R$ in cAMP assays. (A) The change in NECA potency (pEC_{50}) in the presence of 10 μM compound in A_1R-FlpInCHO or $A_{2A}R$-FlpInCHO cells. NECA concentration-response curves for the inhibition of forskolin-stimulated cAMP accumulation in the absence and presence of compound **8** (B) or **19** (C) in A_1R-FlpInCHO cells. Data represent the mean ± SEM from n = 3–4 individual replicates performed in duplicate. Error bars not shown lie within the dimensions of the symbol. $^*p < 0.05$, one-way ANOVA with Dunnett's post-test compared to NECA alone.

compared to the $A_{2A}R$ (Fig. 5B). Gaddum-Schild analysis was performed for **22l** at the A_1R, assessing the influence of increasing concentrations of this compound (0.3–30 μM) on the NECA concentration-response curve (Fig. 5C). Global analysis of the functional interactions preferentially fit to a model of competitive antagonism with an estimated $pK_B = 7.48 \pm 0.09$ (33 nM), a 28-fold improvement of affinity compared to the screening hit. In radioligand binding assays, **22l** displayed an affinity of 7.14 ± 0.02 (72 nM) at the A_1R (Fig. S3). The bulky noradamantane group of **22l** was predicted to occupy the same pocket as the cyclohexane moiety of the co-crystallized ligand DU172 (Fig. 5D).

In the case of compound **19**, the pyridine-3-yl substituent filled the non-conserved pocket, which only resulted in weak subtype selectivity. In order to identify substituents that could improve selectivity, a virtual library of analogs was generated. The library contained molecules in which the pyridine-3-yl of compound **19** was replaced by diverse chemical groups, which could be obtained by amination of a 2-methylsulfoxidepyrimidine derivative (Fig. 6A). A set of 2284 compounds was docked to both the A_1R and $A_{2A}R$, and eight compounds were selected for synthesis based on the predicted binding modes. Briefly, 4-picoline (compound **23**) and thiophene-2-carboxylate ethyl ester reacted under promotion by LiHMDS to provide compound **24**. Heating compound **24** in N,N-dimethylformamide dimethyl acetal afforded the dimethylamino derivative, compound **25**. Condensation of compound **25** with thiourea gave a 2-methylthiopyrimidine derivative compound **26**, which was oxidized by mCPBA to give compound **27**. Amination of compound **27** using the eight selected primary amines afforded the target compounds (**28a-h**). The functional affinities (pK_B) of the compound **19** derivatives at the A_1R and $A_{2A}R$ were determined from functional inhibition cAMP assays, interacting an EC_{80} concentration of agonist against increasing compound concentrations (1 nM–10 μM), with compound affinity values derived using Equations (3)–(5). Six compounds had a significantly greater affinity compared to compound **19**, with four compounds (**28b-c**, **28f**, and **28h**) also having significantly greater affinity for the A_1R compared to the $A_{2A}R$ (Fig. 6B, Table 3, and Fig. S4). Notably, compound **28c** had a low nanomolar affinity with an estimated K_B of 2 nM and 76-fold selectivity for the A_1R over the $A_{2A}R$. Gaddum-Schild analysis was performed for **28c** at the A_1R, assessing the influence of 0.3–30 μM of this compound on the NECA concentration-response curve (Fig. 6C). Global analysis of the functional interactions preferentially fit to a model of competitive antagonism with an estimated $pK_B = 7.84 \pm 0.09$ (14 nM), a 190-fold improvement of affinity compared to the docking hit. Similarly, an affinity of 7.65 ± 0.03 (22 nM) at the A_1R was determined using radioligand binding assays (Fig. S3). Compound **28c** was predicted to position a 3-methyl-tetrahydrofuran moiety in the non-conserved pocket (Fig. 6D).

3. Discussion

Three main results emerged from our structure-based virtual screens for adenosine receptor ligands. First, A_1R antagonists were discovered with a high hit rate and the most potent compounds had submicromolar affinities. Second, docking to structures of the $A_{2A}R$ subtype were carried out to avoid compounds interacting with this closely related receptor. Although several of the screening hits showed the predicted A_1R selectivity, there were only small differences in ligand activity between the two subtypes and several compounds were also potent at the anti-

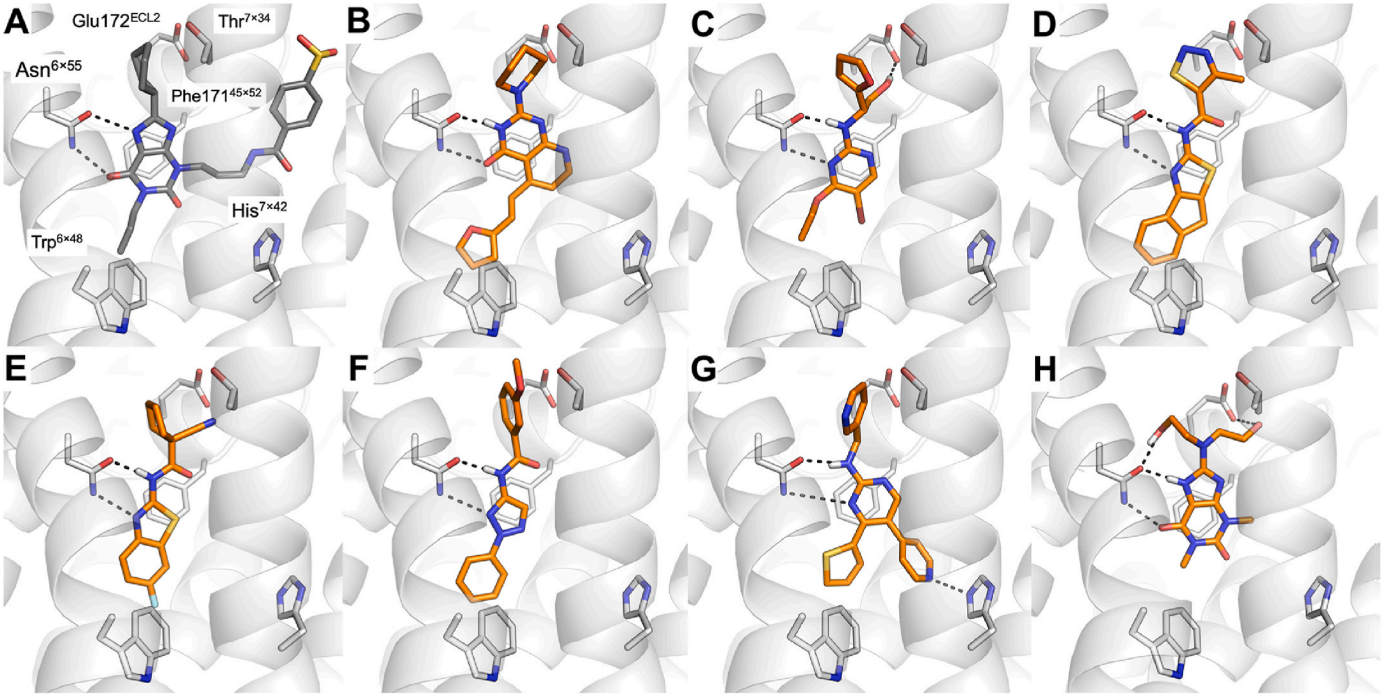

Fig. 4. Predicted binding modes of discovered ligands from the virtual screen. (A) Co-crystallized ligand DU172 (PDB code: 5UEN) (B) **2**, (C) **5**, (D) **8**, (E) **10**, (F) **14**, (G) **19**, and (H) **20**. The A$_1$R is shown as a white cartoon with ligands and selected side chains in sticks. Receptor-ligand hydrogen bonds are shown as black dashed lines.

target. Third, docking of tailored chemical libraries guided hit optimizations, which resulted in antagonists with low nanomolar potency and up to 76-fold subtype selectivity.

The adenosine receptor family has served as a prototypical model for understanding ligand recognition by GPCRs. Together with previous virtual screening studies, our results illustrate the impact of receptor structures on rational ligand discovery. Prior to the determination of the first structure of an adenosine receptor, homology models were used to predict ligand binding modes. Mutagenesis studies had identified the residues involved in ligand recognition, but it remained challenging to predict complexes with high accuracy due to the lack of suitable templates for homology modeling [34]. At this time, a structure-based virtual screen using a homology model of the A$_{2A}$R identified ligands with a hit rate of $\sim$4–9% [35]. Access to a first crystal structure of the A$_{2A}$R clearly improved virtual screening performance with hit rates as high as 45% [14,15,36]. Moreover, the A$_{2A}$R crystal structure could also be used as template to generate more accurate models of other subtypes and virtual screens using these also resulted in improved hit rates. The virtual screening hit rate we achieved with the A$_1$R crystal structure (35%) was similar to that obtained using a homology model [37]. If homology models perform equally well in virtual screening, what is the value of determining structures of other adenosine receptor subtypes? An inherent limitation of homology modeling is the prediction of non-conserved regions of closely related receptors, which will be essential in structure-based design of subtype-selective ligands [38]. In the case of the A$_1$R subtype, the extracellular region that contributes to forming the pocket that we targeted to optimize selectivity was challenging to model based on the A$_{2A}$R structure [37]. The major contribution of access to A$_1$R crystal structures was hence to reveal the location and shape of non-conserved regions.

Models of the receptor-ligand complexes showed how to modify the initial hits in order to further improve potency and selectivity, which allowed us to focus our efforts on a single hot spot of the binding site. Optimization was focused on two virtual screening hits, which represented 2-aminothiazole- (compound **8**) and 2-aminopyrimidine-based (compound **19**) scaffolds that have previously been described as adenosine receptor antagonists [32,39]. By identifying commercial building blocks that could be used to synthesize compounds with diverse substituents, a large virtual chemical library of relevant analogs was generated. Encouragingly, compounds with substantially improved potency and selectivity were identified. Docking was unable to predict the compounds with the best potency, but guided the selection of substituents with an optimal size and polarity among thousands of alternatives. After evaluating 27 analogs, we identified **22l** and **28c**, which have nanomolar A$_1$R affinities and physicochemical properties that satisfy Lipinski's rule of five (Table S3) [40]. Selectivity for the A$_1$R subtype was achieved by replacing the aromatic substituents of compounds **8** and **19** with bulkier aliphatic groups in the subpocket formed by non-conserved residue Thr270$^{7.35}$. The most potent ligand (compound **28c**) displayed 76-fold selectivity for the A$_1$R over the A$_{2A}$R subtype. The fact that many analogs with substituents targeting the right pocket could be synthesized rapidly with standard reactions was a fortuitous result. The efficiency of the approach could hence be optimized by considering synthetic feasibility of analogs already at the compound selection step. Together with the recent release of make-on-demand libraries containing billions of compounds [41], which are often less expensive than the building blocks needed to synthesize analogs, the lead generation step can be further accelerated.

It should be noted that although the predicted ligands were expected to be selective based on the docking screen, the hit rates for the target and anti-target were similar (35 and 45%, respectively). None of the hits from the virtual screen showed strong A$_1$R selectivity and several compounds were even more potent at the A$_{2A}$R subtype. In agreement with our results, previous virtual screening studies found that prediction of selective ligands is challenging even if high resolution crystal structures are available [42,43], which reflects weaknesses of molecular docking methods. One of the major disadvantages of standard docking algorithms is that conformational flexibility and induced fit effects are either neglected or only partially taken into account [44]. In this work, we attempted to improve the description of receptor flexibility by docking to multiple experimental structures of the anti-target. However, despite the fact that each discovered ligand was predicted to fit

Table 2
Affinity and subtype selectivity for compound **8** and analogs at the A_1R and $A_{2A}R$.

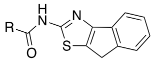

ID	R	pK_B[a]		Subtype selectivity[b] $pK_B(A_1R) - pK_B(A_{2A}R)$
		A_1R	$A_{2A}R$	
8		6.03 ± 0.07	N/A[c]	N/A
22a	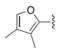	<5.5[d]	N/A	N/A
22b	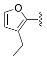	5.93 ± 0.06	N/A	N/A
22c	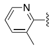	<5.5	N/A	N/A
22d	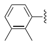	6.67 ± 0.11	<5.5	N/D[e]
22e	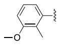	6.20 ± 0.08	<5.5	N/D
22f	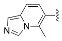	<5.5	<5.5	N/A
22g	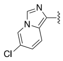	<5.5	N/A	N/A
22h	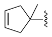	7.57 ± 0.03***	6.42 ± 0.22	1.14 ± 0.19
22i	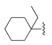	6.86 ± 0.07	6.20 ± 0.21	0.66 ± 0.26
22j		7.71 ± 0.06****	7.28 ± 0.22	0.43 ± 0.23
22k	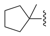	7.86 ± 0.20****	7.40 ± 0.16	0.46 ± 0.26
22l	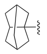	7.57 ± 0.08***	6.30 ± 0.45	1.27 ± 0.46
22m		7.24 ± 0.1**	7.00 ± 0.12	0.24 ± 0.16
22n	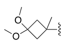	6.70 ± 0.07	7.25 ± 0.13	−0.55 ± 0.15
22o	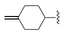	7.70 ± 0.23****	7.03 ± 0.05	0.67 ± 0.24
22p	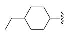	<5.5	<5.5	N/D
22q	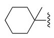	6.19 ± 0.79	6.60 ± 0.02	−0.41 ± 0.79
22r	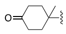	7.85 ± 0.01****	7.25 ± 0.08	0.60 ± 0.13
22s	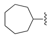	7.29 ± 0.29**	6.87 ± 0.17	0.42 ± 0.34

*$p < 0.05$, **$p < 0.01$, ***$p < 0.001$, ****$p < 0.0001$ one-way ANOVA with Dunnett's post-test significant relative to **8**.

[a] Negative logarithm of the equilibrium dissociation constant (pK_B) for compounds determined from pharmacological assessment in FlpInCHO cells stably expressing the corresponding human receptor. Data represent mean ± standard error (n = 3–4).

[b] Subtype selectivity calculated as $pK_B(A_1R) - pK_B(A_{2A}R)$.

[c] N/A denotes not assessed.

[d] Compound affinity determined as $pK_B < 5.5$ upon incomplete inhibition at the highest concentration assessed.

[e] N/D denotes not determined.

substantially better in the A_1R binding site than in multiple $A_{2A}R$ conformations, the compounds still showed activity at the anti-target. In order to further improve the virtual screening results, it will likely be necessary to use higher level methods to obtain more accurate predictions of binding affinities. For example, molecular dynamics simulations combined with enhanced sampling or free energy methods have the potential to predict binding affinities and this technique was recently applied successfully to the adenosine receptors [45–51]. The computational cost of such methods does not yet allow for the screening of large chemical libraries, but would be feasible to apply in the lead optimization step.

Table 3
Affinity and subtype selectivity for compound **19** and analogs at the A_1R and $A_{2A}R$.

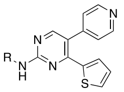

ID	R	pK_B[a]		Subtype Selectivity[b] $pK_B(A_1R) - pK_B(A_{2A}R)$
		A_1R	$A_{2A}R$	
19		5.56 ± 0.08	N/A[c]	N/A
28a	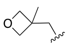	<5.5	<5.5	N/A
28b	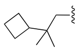	7.15 ± 0.06****	6.09 ± 0.12	1.06 ± 0.13
28c	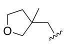	8.64 ± 0.11****	6.76 ± 0.05	1.88 ± 0.12
28d	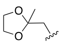	6.38 ± 0.12*	<5.5[d]	N/D[e]
28e	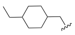	5.96 ± 0.09	<5.5	N/D
28f	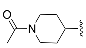	7.82 ± 0.18****	6.57 ± 0.08	1.25 ± 0.20
28g	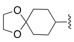	7.07 ± 0.32****	6.53 ± 0.13	0.54 ± 0.35
28h	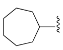	8.1 ± 0.09****	6.79 ± 0.07	1.31 ± 0.11

*$p < 0.05$, **$p < 0.01$, ***$p < 0.001$, ****$p < 0.0001$ one-way ANOVA with Dunnett's post-test significant relative to **19**.

[a] Negative logarithm of the equilibrium dissociation constant (pK_B) for compounds determined from pharmacological assessment in FlpInCHO cells stably expressing the corresponding human receptor. Data represent mean ± standard error (n = 3–4).

[b] Subtype selectivity represents the difference in compound affinity at the two subtypes, $\Delta pK_B = pK_B(A_1R) - pK_B(A_{2A}R)$.

[c] N/A denotes not assessed.

[d] Compound affinity determined as $pK_B < 5.5$ upon incomplete inhibition at the highest concentration assessed.

[e] N/D denotes not determined.

To summarize, our results highlight the potential of structure-based methods to identify and guide optimization of GPCR ligands. The rapidly increasing structural coverage of the GPCR family [2] enables the consideration of multiple targets to take advantage of polypharmacology to enhance therapeutic effects and also avoid interactions with receptors associated with side effects. The approach taken in this work, which combines virtual screening of millions of diverse compounds to identify hits with the generation of focused virtual libraries in the optimization step, can facilitate the development of potent and selective leads.

4. Experimental section

4.1. Molecular docking

Docking screens were carried out with the program DOCK3.6 [27, 52] using an A_1R crystal structure (PDB code: 5UEN) [21] and an ensemble of six diverse $A_{2A}R$ crystal structures (PDB codes: 4EIY [53], 3VGA [54], 3PWH [55], 2YDV [56], 4UG2 [57] and 5G53 [58]). Each structure was prepared by reverting engineered mutations to the WT sequence, adding missing side chains, and removing non-protein atoms. Ionizable residues were set to their most probable protonation state at pH 7. Histidine residues in the binding site were assigned based on visual inspection of hydrogen bonding networks. In the A_1R binding site, $His264^{ECL3}$ and $His278^{7\times42}$ were protonated at the Nδ position whereas $His251^{6\times52}$ was protonated at the Nε position. For the $A_{2A}R$, the corresponding residues were assigned the same protonation states except in the case of $His264^{ECL3}$. Depending on the conformation of ECL3 and

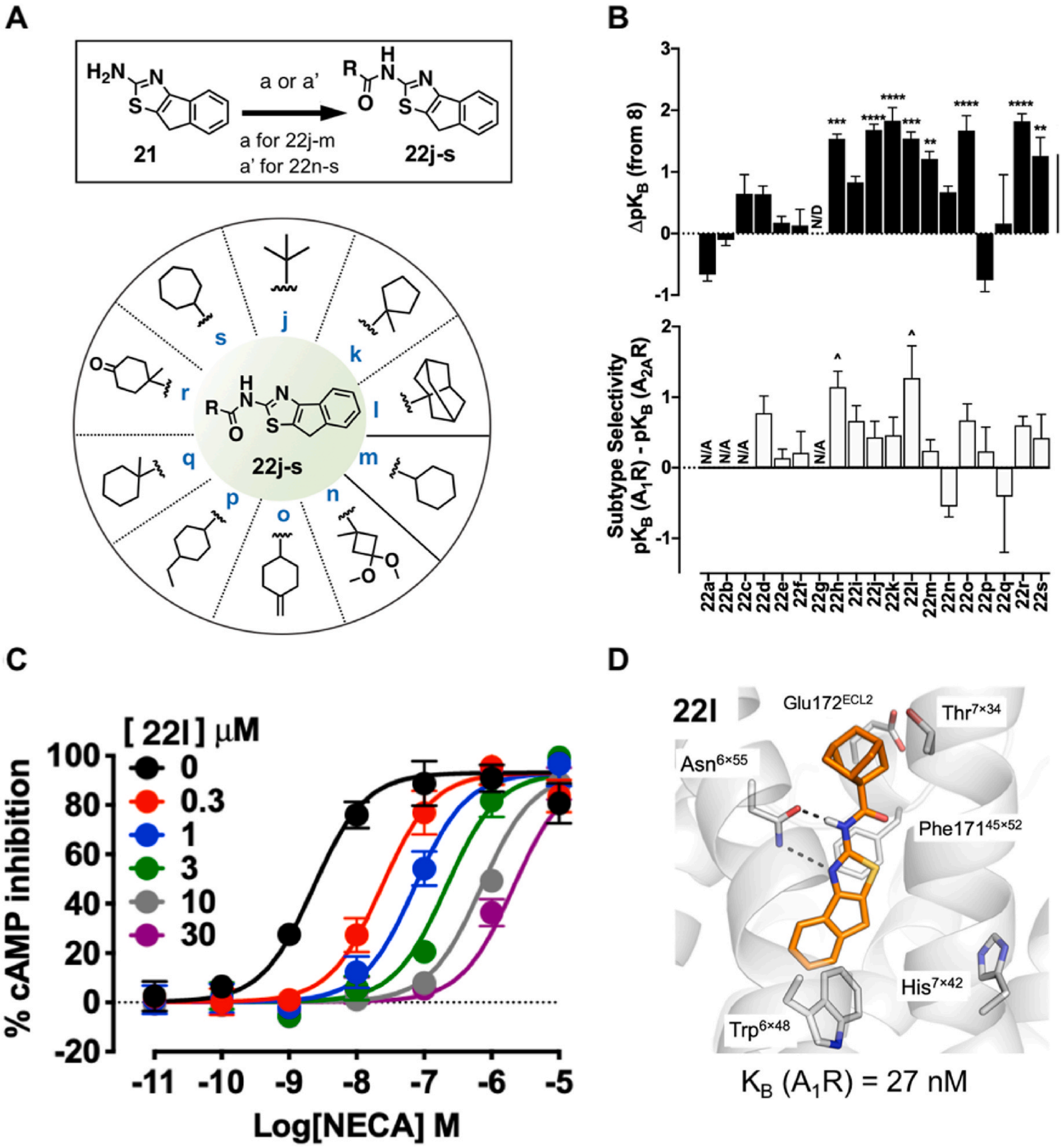

Fig. 5. Structure-guided optimization of compound **8**. (**A**) Tailored chemical libraries were generated based on commercially available building blocks. Synthesis of selected analogs used (a) RCOCl, pyridine, 0 °C - rt, 30 min, 44–56% (hplc) for **22j-m**. (a') RCOOH, HATU, NMP, 90 °C, overnight, 35–51% (hplc) for compounds **22n-s**. (**B**) Pharmacological assessment of derivates of compound **8** at the A_1R and $A_{2A}R$ in cAMP assays. Data show the change in A_1R affinity (ΔpK_B) relative to compound **8** (top panel) and the compound subtype selectivity for the A_1R relative to the $A_{2A}R$, calculated as $pK_B(A_1R)$ - $pK_B(A_{2A}R)$ (bottom panel). Data represent the mean ± SEM from n = 3–4 individual replicates performed in duplicate. N/D denotes not determined; N/A denotes not assessed; $^*p < 0.05$, $^{**}p < 0.01$, $^{***}p < 0.001$, $^{****}p < 0.0001$ one-way ANOVA with Dunnett's post-test relative to the pK_B for compound **8**; $\hat{}p < 0.05$, multiple *t*-test comparing corresponding pK_B values for the A_1R and $A_{2A}R$ with the Holm-Šídák method used to correct for multiple comparisons. (**C**) A_1R antagonism mediated by compound **22l**, the most selective analog of compound **8**. NECA concentration-response curves for the inhibition of forskolin-stimulated cAMP accumulation in the absence and presence of compound **22l** in A_1R-FlpInCHO cells. Data represent the mean ± SEM from n = 4 individual replicates performed in duplicate. Error bars not shown lie within the dimensions of the symbol. (**D**) Predicted binding mode of compound **22l**. The A_1R is represented as grey cartoons with selected side chains and the ligand shown with sticks. Receptor-ligand hydrogen bonds are shown as black dashed lines.

interactions with $Glu169^{ECL2}$, this residue was either protonated at both Nδ and Nε (PDB codes: 4EIY [53], 2YDV [56], 4UG2 [57], and 5G53 [58]) or only at the Nδ position (3VGA [54] and 3PWH [55]).

The flexible ligand sampling algorithm of DOCK3.6 superimposes rigid parts of the docked compounds onto binding site matching spheres that define putative positions of ligand atoms [52]. A set of 45 matching spheres were used for each receptor structure. Atoms of the co-crystallized ligands in the vicinity of $Asn^{6.55}$ were used as starting point for generation of the matching spheres in the A_1R and $A_{2A}R$ structures. Ligand sampling in DOCK3.6 is determined by the bin size, overlap, and distance tolerance threshold, which were set to 0.4, 0.3, and 1.5 Å in the A_1R screens. The same parameters were set to 0.4, 0.1, and 1.5 Å in the $A_{2A}R$ screens. Each docked ligand conformation that did not result in clashes with the receptor was scored using a physics-based scoring function. The binding energy was calculated as the sum of the receptor-ligand electrostatic and van der Waals interactions, corrected

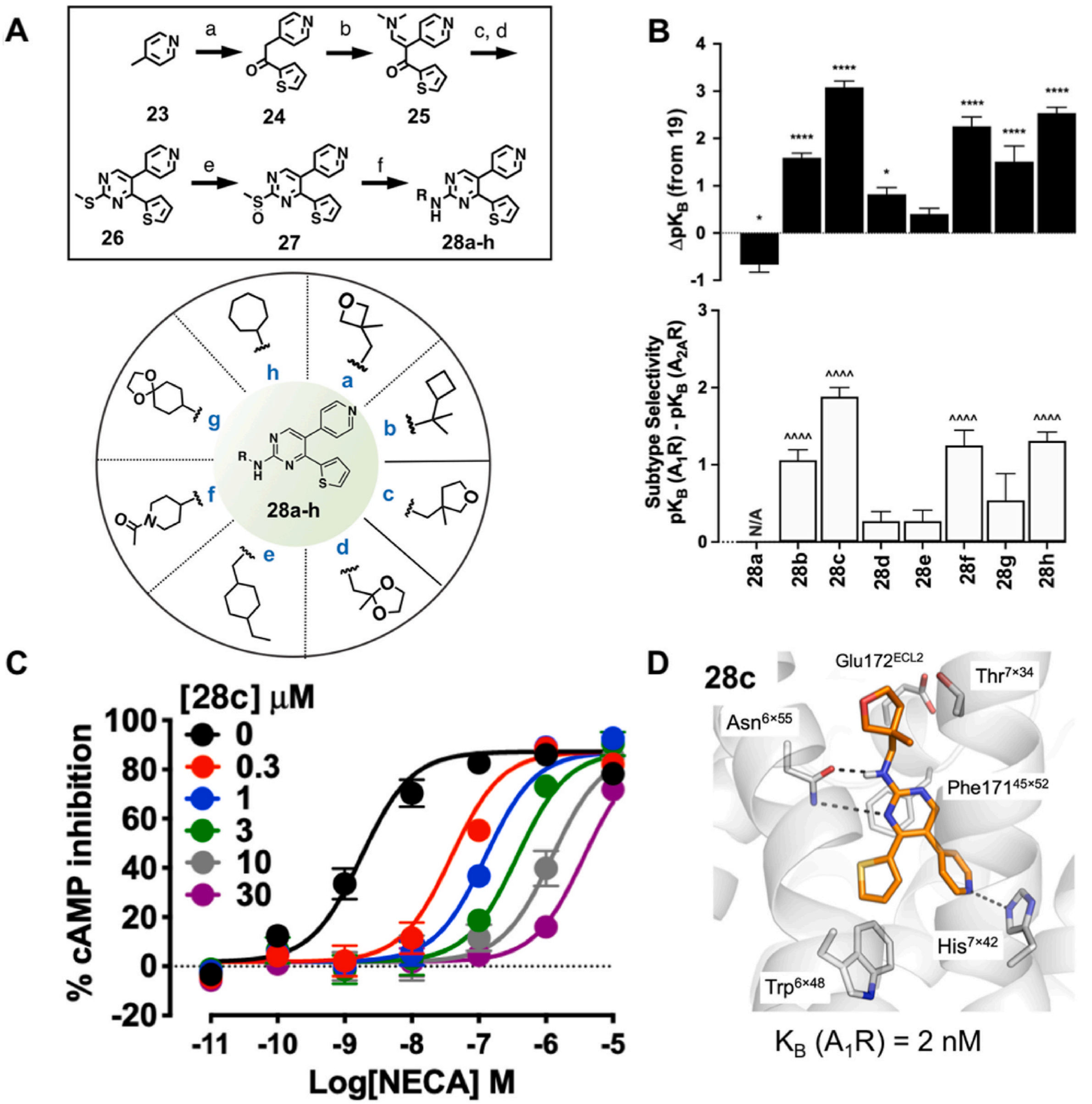

Fig. 6. Structure-guided optimization of compound **19**. (**A**) Tailored chemical libraries were generated based on commercially available building blocks. Synthesis of the selected analogs used (a) LiHMDS, thiophene-2-carboxylate ethyl ester, THF, 1 h, 89%. (b) $Me_2NCH(OMe)_2$ 100 °C, 2 h. (c) thiourea, tBuOK, EtOH, 100 °C, 1 h. (d) MeI, DCM, rt, 30 min, 38% (3 steps). (e) mCPBA, DCM, 0 °C – rt, 2 h, 60%. (f) RNH_2, THF, 50 °C, overnight, 21–91% (hplc). (**B**) Pharmacological assessment of derivatives of compound **19** at the A_1R and $A_{2A}R$ in cAMP assays. Data show the change in A_1R affinity (ΔpK_B) relative to compound **19** (top panel) and the compound subtype selectivity for the A_1R relative to the $A_{2A}R$, calculated as pK_B (A_1R) - pK_B ($A_{2A}R$) (bottom panel). Data represent the mean ± SEM from $n = 4$ individual replicates performed in duplicate. N/A denotes not assessed; $^*p < 0.05$, $^{**}p < 0.01$, $^{***}p < 0.001$, $^{****}p < 0.0001$ one-way ANOVA with Dunnett's post-test significant relative to the pK_B for compound **19**; $^\wedge p < 0.05$, $^{\wedge\wedge}p < 0.01$, $^{\wedge\wedge\wedge}p < 0.001$, $^{\wedge\wedge\wedge\wedge}p < 0.0001$ multiple *t*-test comparing corresponding pK_B values for the A_1R and $A_{2A}R$ with the Holm-Šídák method used to correct for multiple comparisons. (**C**) A_1R antagonism mediated by compound **28c**, the highest affinity and most selective analog of compound **19**. NECA concentration-response curves for the inhibition of forskolin-stimulated cAMP accumulation in the absence and presence of compound **28c** in A_1R-FlpInCHO cells. Data represent the mean ± SEM from $n = 4$ individual replicates performed in duplicate. Error bars not shown lie within the dimensions of the symbol. (**D**) Predicted binding mode of compound **28c**. The A_1R is represented as grey cartoons with selected side chains and the ligand shown as sticks. Receptor-ligand hydrogen bonds are shown as black dashed lines.

for ligand desolvation [27]. These energy terms were calculated from pre-calculated grids. The electrostatic and van der Waals grids were based on the AMBER force field. The electrostatic potential in the binding site was calculated using the program Delphi with dielectric constants of 2 and 78 representing protein and water environments, respectively. Hydrogen bonding between $Asn^{6.55}$ and the docked compounds was favored by increasing the dipole moment of the side chain, as described previously [15]. The van der Waals grid was generated using the program CHEMGRID. For the top scoring conformation of each docked compound, 100 steps of rigid-body minimization were carried out.

4.2. Compound databases

A library of 4.6 million lead-like compounds (250 Da ≤ MW ≤ 350 Da, calculated LogP ≤3.5, and ≤7 rotatable bonds) was downloaded from ZINC (accessed 25/09/2014), which is a free database of commercially available compounds for virtual screening [59,60]. In hit optimization, commercially available libraries and virtual chemical libraries with analogs of compounds **8** and **19** were considered. The virtual libraries were generated by identifying commercially available building blocks compatible with relevant reactions (amide coupling and amination, Figs. 5 and 6). Compared to the lead-like ZINC library, larger and more hydrophobic compounds were included in these libraries and additional filters were added to obtain drug-like ligands (MW ≤ 400 Da, calculated LogP ≤4, ≤3 aromatic rings, ≤5 hydrogen bond acceptors, ≤4 hydrogen bond donors, ≤6 rotatable bonds, <2 chiral centers, and only neutral compounds). The virtual chemical libraries were prepared using Openeye toolkits (OpenEye Toolkits 2020.2.0 OpenEye Scientific Software, Santa Fe, NM. http://www.eyesopen.com) and the ZINC database protocol. After docking of the analogs, compounds were selected among the top-ranked compounds (typically ~500 molecules). None of the experimentally tested compounds contained any motifs present in pan-assay interference compounds, which was evaluated using the ZINC20 database tools (http://zinc20.docking.org/patterns/home/).

4.3. 2D similarity and physicochemical properties

2D similarity to known A_1R and $A_{2A}R$ ligands from the ChEMBL [28–30] and IUPHAR/BPS Guide to Pharmacology databases [31] (affinity <10 μM) was calculated using the Tanimoto similarity coefficient (T_c) and Morgan2 fingerprints (1024 bits). Similarity and physicochemical properties were calculated using RDKit (http://www.rdkit.org).

4.4. Compound synthesis

All reagents were purchased from Fluorochem, Sigma-Aldrich, Enamine and Chemtronica. For solvents, DCM, methanol, DMF, and acetonitrile (99.9%) were purchased from VWR International AB, whereas THF was purchased from Sigma-Aldrich. Reagents and solvents were used as such without further purification. All reactions involving air or moisture-sensitive reagents or intermediates were performed under a nitrogen atmosphere. LC-MS was used for monitoring reactions and assessing purity using an Agilent 1100 series HPLC having a C18 Atlantis T3 column (3.0 × 50 mm, 5 μm). Acetonitrile–water (flow rate 0.75 mL/min over 6 min) was used as mobile phase and a Waters micromass Z_Q (model code: MM1) mass spectrometer with electrospray ionization mode was used for detection of molecular ions. TLC silica gel 60 F_{254} plates from Merck were also used in some cases to monitor reactions and particularly during purification of compounds. Visualization of the developed TLC plates was done using UV light (254 nm) and staining with ninhydrin stain or anisaldehyde stain. After workup, organic phases were dried over $Na_2SO_4/MgSO_4$ and filtered before being concentrated under reduced pressure. Silica gel (Matrex, 60 Å, 35–70 μm, Grace Amicon) was used for purification of intermediate compounds with flash column chromatography. ^1H and ^{13}C NMR spectra for synthesized compounds were recorded at 298 K on an Agilent Technologies 400 NMR spectrometer at 400 MHz or 100 MHz, or on Bruker Avance Neo spectrometers at 500 MHz or 125 MHz. Chemical shifts are reported in parts per million (ppm, δ) referenced to the residual ^1H resonance of the solvent ($(CD_3)_2CO$, δ 2.05; $CDCl_3$, δ 7.26; CD_3OD δ 3.31; DMSO-d_6 δ 2.50). Splitting patterns are designated as follows: s (singlet), d (doublet), t (triplet) and m (multiplet), br (broad). Coupling constants (J values) are listed in hertz (Hz). Preparative reversed-phase HPLC was performed on a Kromasil C8 column (250 × 21.2 mm, 5 μm) on a Gilson HPLC equipped with a Gilson 322 pump, a UV/Visible-156 detector and a 202 collector using acetonitrile-water gradients as eluents with a flow rate of 15 mL/min and detection at 210 or 254 nm. Unless otherwise stated, all the tested compounds were purified by HPLC. The purity of the synthesized compounds was ≥95% as determined by high resolution ^1H NMR spectroscopy (500 MHz) and LC-MS.

4.5. Materials

Chinese hamster ovary (CHO) Flp-IN™ (FlpInCHO) cells, Dulbecco's modified Eagle's medium (DMEM) and hygromycin B (Hygrogold™) were purchased from Invitrogen (Carlsbad, CA). DMEM high glucose medium was purchased from Sigma-Aldrich. Fetal bovine serum (FBS) was purchased from ThermoTrace (Melbourne, VIC, Australia). Adenosine deaminase (ADA) was purchased from Roche (Basel, Switzerland). AlphaScreen™ reagents, OptiPhase Supermix™ scintillation cocktail and [^{3}H]DPCPX (8-cyclopentyl-1,3-dipropylxanthine, [dipropyl-2,3-3H (N)]; specific activity, 120 Ci/mmol) were purchased from PerkinElmer (Boston, MA). SLV320 ((*trans*-4-[(2-Phenyl-7H-pyrrolo [2,3-d] pyrimidin-4-yl)amino]cyclohexanol)) was purchased from Tocris Bioscience (Bristol, UK). Compounds **1**–**20** and **22a-i** were purchased from commercial vendors. All other reagents were purchased from Sigma-Aldrich and Tocris and were of analytical grade.

4.6. Cell culture

FlpInCHO cells stably transfected with human A_1R (A_1R-FlpInCHO) or human $A_{2A}R$ ($A_{2A}R$-FlpInCHO) were generated as previously described [9,61]. Cells were maintained in DMEM supplemented with 10% FBS and 500 μg/mL hygromycin-B, and were grown at 37 °C in a humidified incubator containing 5% CO_2.

4.7. cAMP accumulation assay

A_1R-FlpInCHO or $A_{2A}R$-FlpInCHO were seeded into transparent 96-well plates at 20,000 cells/well and incubated for 16–20 h in a humidified incubator at 37 °C in 5% CO_2. On the day of assay, media was removed from wells and replaced with cAMP stimulation buffer (140 mM NaCl, 5 mM KCl, 0.8 μM $MgSO_4$, 0.2 mM Na_2HPO_4, 0.44 mM KH_2PO_4, 1.3 mM $CaCl_2$, 5.6 mM D-glucose, 5 mM HEPES, 0.1% bovine serum albumin (BSA), 1 U/mL ADA and 10 μM rolipram, pH 7.45). Compounds, either at single concentration (10 μM) or concentration range for full interaction/selectivity studies (0.1 nM–30 μM) were added and plates were incubated for 30–60 min at 37 °C in a humidified chamber. Cells were then exposed to NECA, at increasing concentrations (0.01 nM–1 μM) or an EC_{80} concentration (A_1R: 4 nM; $A_{2A}R$: 10 nM) in the presence (A_1R-FlpInCHO) or absence ($A_{2A}R$-FlpInCHO) of 3 μM forskolin. After 30 min incubation at 37 °C, the reaction was terminated by rapid removal of buffer and the addition of 50 μL/well cold ethanol. Following ethanol evaporation, the precipitate was re-suspended in 50 μL/well lysis buffer (0.1% BSA, 0.3% Tween-20, 5 mM HEPES, in MQ water; pH 7.45) and detection of cAMP was performed using LANCE® cAMP Assay kits (PerkinElmer; Boston, MA) and fluorescence measured using an EnVision® plate reader (PerkinElmer; Boston, MA) with standard AlphaScreen™ settings. Agonist concentration-response curves were normalized to the response mediated by 3 μM forskolin or buffer alone.

4.8. Radioligand displacement assays

The A_1R binding affinity of compounds was assessed in whole cell equilibrium binding as previously described [62]. Briefly, A_1R-FlpInCHO cells were seeded into a transparent 96-well plate at 40,000 cells/well in DMEM containing 10% FBS. Following 8 h incubation in a humidified environment at 37 °C in 5% CO_2, cells were washed and maintained in serum free DMEM for approximately 18 h at 37 °C in 5% CO_2. [^{3}H]DPCPX competition binding on intact A_1R-FlpInCHO cells were performed at 4 °C for 12 h in a final volume of 100 μL HEPES buffer (145 mM NaCl, 10 mM D-Glucose, 5 mM KCl, 1 mM $MgSO_4$, 10 mM HEPES, 1.3 mM $CaCl_2$, 15 mM $NaHCO_3$, pH 7.45) containing approximately 1 nM [^{3}H]DPCPX in the presence of increasing concentrations of the compound (0.3 nM-10 μM). Non-specific binding was defined in the presence of a saturating concentration (1 μM) of the high-affinity A_1R antagonist, SLV320. Assays were terminated by washing twice with 100 μL/well cold phosphate buffered saline (PBS), followed by the addition of 100 μL OptiPhase Supermix™ scintillation cocktail and bound radioactivity measured using a MicroBeta^{2}™ plate counter (PerkinElmer).

4.9. Data analysis

Data were analyzed using GraphPad Prism 8.4.3 (GraphPad Software, San Diego, CA). Statistical analysis was performed using a one-way ANOVA with significance defined as $P < 0.05$. NECA concentration-response curves from cAMP accumulation assays in the absence or presence of compounds were fitted to the following three-parameter Hill equation to derive potency estimates:

$$Response = Basal + \frac{(E_{max} - Basal) \times [A]}{EC_{50} + [A]} \tag{1}$$

where EC_{50} is the concentration of NECA (A) in the absence or presence of compounds that gives the midpoint response between basal and maximal effect (E_{max}), which are the lower and upper asymptotes of the response, respectively.

Global fits for functional interaction studies between NECA and multiple concentrations of compounds were fitted to the following competitive model:

$$Response = Bottom + \frac{(E_{max} - bottom)}{1 + \left(\frac{10^{-pEC_{50}}\left[1+\left(\frac{[B]}{10^{-pA_2}}\right)^{S}\right]}{[A]}\right)^{HillSlope}} \tag{2}$$

where pEC_{50} is the negative logarithm of the EC_{50} of NECA (A) in the absence of antagonist (B). HillSlope is the slope of the agonist curve, S is the Schild slope, and pA_2 is the negative logarithm of the molar concentration of antagonist necessary to shift the agonist EC_{50} by a factor of two. When the Schild slope is not significantly different from 1, the pA_2 is equal to the pK_B of the antagonist.

Functional inhibition assays interacting a single concentration of agonist against increasing compound concentrations determined the functional affinity (pK_B) of the compounds at the A_1R and $A_{2A}R$ according to the following set of equations (Prism 8).

$$Response = \frac{E_{max} \times [IC_{50}]}{[IC_{50}] + [B]} \tag{3}$$

where IC_{50} reflects the molar concentration of compound [B] required to decrease by 50% the response mediated by the fixed molar concentration of NECA used for the functional inhibition in the absence of compound (E_{max}). To obtain the molar concentration of NECA that, in the absence of antagonist, mediates the same response level as the IC_{50} from the functional inhibition curve (EC_F), NECA concentration-response curves performed simultaneously to the functional inhibition were analyzed according to the following equation:

$$EC_F = EC_{50}\left(\frac{F}{100 - F}\right) \tag{4}$$

where the EC_{50} is calculated using Eq. (1) and F represents the percentage response from the normalized concentration-response curve that is 50% of that mediated by the fixed molar concentration of NECA used within the functional inhibition assay. Equilibrium dissociation constants (K_B) for the compounds were subsequently estimated by substituting the IC_{50} and EC_F values obtained from Eqs. 3 and 4 into a modified form of the Gaddum equation as described by Lazareno and Birdsall [63].

$$K_B = \frac{IC_{50}}{{[A]}/{EC_F} - 1} \tag{5}$$

Declaration of competing interest

The authors declare that they have no known competing financial interests or personal relationships that could have appeared to influence the work reported in this paper.

Data availability

Data will be made available on request.

Acknowledgements

J.C. received funding from the European Research Council (ERC) under the European Union's Horizon 2020 research and innovation programme (grant agreement: 715052), the Swedish Research Council (VR, grants: 2017-4676 and 2021-4186), and the Swedish Strategic Research Program eSSENCE. This work was also supported by the National Health and Medical Research Council of Australia (NHMRC) project grants: APP1145420 (L T M., A.C.), APP1147291 (L.T.M.). L.T. M. is an Australian National Heart Foundation Future Leaders Fellow. The computations were enabled by resources provided by the Swedish National Infrastructure for Computing (SNIC) at NSC and UPPMAX, partially funded by the Swedish Research Council through grant agreement no. 2018–05973. This study made use of the NMR Uppsala infrastructure, which is funded by the Department of Chemistry—BMC and the Disciplinary Domain of Medicine and Pharmacy. We thank OpenEye Scientific Software for the use of OEToolKits at no cost.

Appendix A. Supplementary data

Supplementary data to this article can be found online at https://doi.org/10.1016/j.ejmech.2023.115419.

References

[1] A.S. Hauser, M.M. Attwood, M. Rask-Andersen, H.B. Schiöth, D.E. Gloriam, Trends in GPCR drug discovery: new agents, targets and indications, Nat. Rev. Drug Discov. 16 (2017) 829–842, https://doi.org/10.1038/nrd.2017.178.

[2] M. Congreve, C. de Graaf, N.A. Swain, C.G. Tate, Impact of GPCR structures on drug discovery, Cell 181 (2020) 81–91, https://doi.org/10.1016/j.cell.2020.03.003.

[3] J.A. Allen, B.L. Roth, Strategies to discover unexpected targets for drugs active at G protein-coupled receptors, Annu. Rev. Pharmacol. Toxicol. 51 (2011) 117–144, https://doi.org/10.1146/annurev-pharmtox-010510-100553.

[4] R.K. Harrison, Phase II and phase III failures: 2013-2015, Nat. Rev. Drug Discov. 15 (2016) 817–818, https://doi.org/10.1038/nrd.2016.184.

[5] M. Michino, T. Beuming, P. Donthamsetti, A.H. Newman, J.A. Javitch, L. Shi, What can crystal structures of aminergic receptors tell us about designing subtype-selective ligands? Pharmacol. Rev. 67 (2015) 198–213, https://doi.org/10.1124/pr.114.009944.

[6] B.B. Fredholm, A.P. Ijzerman, K.A. Jacobson, K.N. Klotz, J. Linden, International Union of Pharmacology. XXV, Nomenclature and classification of adenosine receptors, Pharmacol. Rev. 53 (2001) 527–552.

[7] S.M. McNeill, J.A. Baltos, P.J. White, L.T. May, Biased agonism at adenosine receptors, Cell. Signal. 82 (2021), 109954, https://doi.org/10.1016/j.cellsig.2021.109954.

[8] E.A. Vecchio, C.H. Chuo, J.A. Baltos, L. Ford, P.J. Scammells, B.H. Wang, A. Christopoulos, P.J. White, L.T. May, The hybrid molecule, VCP746, is a potent adenosine A_{2B} receptor agonist that stimulates anti-fibrotic signalling, Biochem. Pharmacol. 117 (2016) 46–56, https://doi.org/10.1016/j.bcp.2016.08.007.

[9] J.A. Baltos, K.J. Gregory, P.J. White, P.M. Sexton, A. Christopoulos, L.T. May, Quantification of adenosine A_1 receptor biased agonism: implications for drug discovery, Biochem. Pharmacol. 99 (2016) 101–112, https://doi.org/10.1016/j.bcp.2015.11.013.

[10] C. Avet, A. Mancini, B. Breton, C. Le Gouill, A.S. Hauser, C. Normand, H. Kobayashi, F. Gross, M. Hogue, V. Lukasheva, S. St-Onge, M. Carrier, M. Héroux, S. Morissette, E.B. Fauman, J.-P. Fortin, S. Schann, X. Leroy, D.E. Gloriam, M. Bouvier, Effector membrane translocation biosensors reveal G protein and βarrestin coupling profiles of 100 therapeutically relevant GPCRs, Elife 11 (2022), e74101, https://doi.org/10.7554/eLife.74101.

[11] A. Inoue, F. Raimondi, F.M.N. Kadji, G. Singh, T. Kishi, A. Uwamizu, Y. Ono, Y. Shinjo, S. Ishida, N. Arang, K. Kawakami, J.S. Gutkind, J. Aoki, R.B. Russell, Illuminating G-protein-coupling selectivity of GPCRs, Cell 177 (2019) 1933–1947, https://doi.org/10.1016/j.cell.2019.04.044.

[12] J.F. Chen, H.K. Eltzschig, B.B. Fredholm, Adenosine receptors as drug targets-what are the challenges? Nat. Rev. Drug Discov. 12 (2013) 265–286, https://doi.org/10.1038/nrd3955.

[13] V.P. Jaakola, M.T. Griffith, M.A. Hanson, V. Cherezov, E.Y.T. Chien, J.R. Lane, A. P. Ijzerman, R.C. Stevens, The 2.6 angstrom crystal structure of a human A_{2A} adenosine receptor bound to an antagonist, Science 322 (2008) 1211–1217, https://doi.org/10.1126/science.1164772.

[14] J. Carlsson, L. Yoo, Z.G. Gao, J.J. Irwin, B.K. Shoichet, K.A. Jacobson, Structure-based discovery of A_{2A} adenosine receptor ligands, J. Med. Chem. 53 (2010) 3748–3755, https://doi.org/10.1021/jm100240h.

[15] D. Rodríguez, Z.G. Gao, S.M. Moss, K.A. Jacobson, J. Carlsson, Molecular docking screening using agonist-bound GPCR structures: probing the A_{2A} adenosine receptor, J. Chem. Inf. Model. 55 (2015) 550–563, https://doi.org/10.1021/ci500639g.

[16] F. Ballante, A. Rudling, A. Zeifman, A. Luttens, D.D. Vo, J.J. Irwin, J. Kihlberg, J. Brea, M.I. Loza, J. Carlsson, Docking finds GPCR ligands in dark chemical matter, J. Med. Chem. 63 (2020) 613–620, https://doi.org/10.1021/acs.jmedchem.9b01560.

[17] M. Jaiteh, A. Zeifman, M. Saarinen, P. Svenningsson, J. Bréa, M.I. Loza, J. Carlsson, Docking screens for dual inhibitors of disparate drug targets for Parkinson's disease, J. Med. Chem. 61 (2018) 5269–5278, https://doi.org/10.1021/acs.jmedchem.8b00204.

[18] A. Borodovsky, C.M. Barbon, Y. Wang, M. Ye, L. Prickett, D. Chandra, J. Shaw, N. Deng, K. Sachsenmeier, J.D. Clarke, B. Linghu, G.A. Brown, J. Brown, M. Congreve, R.K. Cheng, A.S. Dore, E. Hurrell, W. Shao, R. Woessner, C. Reimer, L. Drew, S. Fawell, A.G. Schuller, D.A. Mele, Small molecule AZD4635 inhibitor of A2AR signaling rescues immune cell function including CD103+ dendritic cells enhancing anti-tumor immunity, J. Immunother. Cancer. 8 (2020), e000417, https://doi.org/10.1136/jitc-2019-000417.

[19] D. Charvin, R. Medori, R.A. Hauser, O. Rascol, Therapeutic strategies for Parkinson disease: beyond dopaminergic drugs, Nat. Rev. Drug Discov. 17 (2018) 804–822, https://doi.org/10.1038/nrd.2018.136.

[20] F. Ballante, A.J. Kooistra, S. Kampen, C. de Graaf, J. Carlsson, Structure-based virtual screening for ligands of G protein–coupled receptors: what can molecular docking do for you? Pharmacol. Rev. 73 (2021) 1698–1736, https://doi.org/10.1124/PHARMREV.120.000246.

[21] A. Glukhova, D.M. Thal, A.T. Nguyen, E.A. Vecchio, M. Jörg, P.J. Scammells, L. T. May, P.M. Sexton, A. Christopoulos, Structure of the adenosine A_1 receptor reveals the basis for subtype selectivity, Cell 168 (2017) 867–877, https://doi.org/10.1016/j.cell.2017.01.042.

[22] R.K.Y. Cheng, E. Segala, N. Robertson, F. Deflorian, A.S. Doré, J.C. Errey, C. Fiez-Vandal, F.H. Marshall, R.M. Cooke, Structures of human A_1 and A_{2A} adenosine receptors with xanthines reveal determinants of selectivity, Structure 25 (2017) 1275–1285, https://doi.org/10.1016/j.str.2017.06.012.

[23] B. Hocher, Adenosine A_1 receptor antagonists in clinical research and development, Kidney Int. 78 (2010) 438–445, https://doi.org/10.1038/ki.2010.204.

[24] B.J. Bender, S. Gahbauer, A. Luttens, J. Lyu, C.M. Webb, R.M. Stein, E.A. Fink, T. E. Balius, J. Carlsson, J.J. Irwin, B.K. Shoichet, A practical guide to large-scale docking, Nat. Protoc. 16 (2021) 4799–4832, https://doi.org/10.1038/s41596-021-00597-z.

[25] B. Carpenter, G. Lebon, Human adenosine A_{2A} receptor: molecular mechanism of ligand binding and activation, Front. Pharmacol. 8 (2017) 898, https://doi.org/10.3389/fphar.2017.00898.

[26] V. Isberg, C. De Graaf, A. Bortolato, V. Cherezov, V. Katritch, F.H. Marshall, S. Mordalski, J.P. Pin, R.C. Stevens, G. Vriend, D.E. Gloriam, Generic GPCR residue numbers - aligning topology maps while minding the gaps, Trends Pharmacol. Sci. 36 (2015) 22–31, https://doi.org/10.1016/j.tips.2014.11.001.

[27] M.M. Mysinger, B.K. Shoichet, Rapid context-dependent ligand desolvation in molecular docking, J. Chem. Inf. Model. 50 (2010) 1561–1573, https://doi.org/10.1021/ci100214a.

[28] D. Mendez, A. Gaulton, A.P. Bento, J. Chambers, M. De Veij, E. Félix, M. P. Magariños, J.F. Mosquera, P. Mutowo, M. Nowotka, M. Gordillo-Marañón, F. Hunter, L. Junco, G. Mugumbate, M. Rodriguez-Lopez, F. Atkinson, N. Bosc, C. J. Radoux, A. Segura-Cabrera, A. Hersey, A.R. Leach, ChEMBL: towards direct deposition of bioassay data, Nucleic Acids Res. 47 (2019) D930–D940, https://doi.org/10.1093/nar/gky1075.

[29] A. Gaulton, A. Hersey, M.L. Nowotka, A. Patricia Bento, J. Chambers, D. Mendez, P. Mutowo, F. Atkinson, L.J. Bellis, E. Cibrian-Uhalte, M. Davies, N. Dedman, A. Karlsson, M.P. Magarinos, J.P. Overington, G. Papadatos, I. Smit, A.R. Leach, The ChEMBL database in 2017, Nucleic Acids Res. 45 (2017) D945–D954, https://doi.org/10.1093/nar/gkw1074.

[30] A.P. Bento, A. Gaulton, A. Hersey, L.J. Bellis, J. Chambers, M. Davies, F.A. Krüger, Y. Light, L. Mak, S. McGlinchey, M. Nowotka, G. Papadatos, R. Santos, J. P. Overington, The ChEMBL bioactivity database: an update, Nucleic Acids Res. 42 (2014) D1083–D1090, https://doi.org/10.1093/nar/gkt1031.

[31] S.P.H. Alexander, et al., The concise guide to pharmacology 2021/22: G protein-coupled receptors, Br. J. Pharmacol. 178 (2021), https://doi.org/10.1111/bph.15538. S27–S156.

[32] B.B. Fredholm, A.P. Ijzerman, K.A. Jacobson, J. Linden, C.E. Müller, International union of basic and clinical pharmacology. LXXXI. Nomenclature and classification of adenosine receptors - an update, Pharmacol. Rev. 63 (2011) 1–34, https://doi.org/10.1124/pr.110.003285.

[33] A. Göblyös, S.N. Santiago, D. Pietra, T. Mulder-Krieger, J.V.F.D. Künzel, J. Brussee, A.P. Ijzerman, Synthesis and biological evaluation of 2-aminothiazoles and their amide derivatives on human adenosine receptors. Lack of effect of 2-aminothiazoles as allosteric enhancers, Bioorganic Med. Chem. 13 (2005) 2079–2087, https://doi.org/10.1016/j.bmc.2005.01.006.

[34] M. Michino, E. Abola, C.L. Brooks, J.S. Dixon, J. Moult, R.C. Stevens, Community-wide assessment of GPCR structure modeling and docking understanding, Nat. Rev. Drug Discov. 8 (2009) 455–463, https://doi.org/10.1038/nrd2877.Community-wide.

[35] C.J. Langmead, S.P. Andrews, M. Congreve, J.C. Errey, E. Hurrell, F.H. Marshall, J. S. Mason, C.M. Richardson, N. Robertson, A. Zhukov, M. Weir, Identification of novel adenosine A_{2A} receptor antagonists by virtual screening, J. Med. Chem. 55 (2012) 1904–1909, https://doi.org/10.1021/jm201455y.

[36] V. Katritch, V.P. Jaakola, J.R. Lane, J. Lin, A.P. Ijzerman, M. Yeager, I. Kufareva, R. C. Stevens, R. Abagyan, Structure-based discovery of novel chemotypes for adenosine A_{2A} receptor antagonists, J. Med. Chem. 53 (2010) 1799–1809, https://doi.org/10.1021/jm901647p.

[37] P. Kolb, K. Phan, Z.G. Gao, A.C. Marko, A. Sali, K.A. Jacobson, Limits of ligand selectivity from docking to models: in silico screening for A_1 adenosine receptor antagonists, PLoS One (2012), e49910, https://doi.org/10.1371/journal.pone.0049910.

[38] D. Rodríguez, J. Brea, M.I. Loza, J. Carlsson, Structure-based discovery of selective serotonin 5-HT_{1B} receptor Ligands, Structure 22 (2014) 1140–1151, https://doi.org/10.1016/j.str.2014.05.017.

[39] A.P. Ijzerman, K.A. Jacobson, C.E. Müller, B.N. Cronstein, R.A. Cunha, International union of basic and clinical pharmacology. CXII: adenosine receptors: a further update, Pharmacol. Rev. 74 (2022) 340–372, https://doi.org/10.1124/pharmrev.121.000445.

[40] C.A. Lipinski, F. Lombardo, B.W. Dominy, P.J. Feeney, Experimental and computational approaches to estimate solubility and permeability in drug discovery and development settings, Adv. Drug Deliv. Rev. 64 (2012) 4–17, https://doi.org/10.1016/j.addr.2012.09.019.

[41] T. Hoffmann, M. Gastreich, The next level in chemical space navigation: going far beyond enumerable compound libraries, Drug Discov. Today (2019) 1148–1156, https://doi.org/10.1016/j.drudis.2019.02.013.

[42] A.C. Kruse, D.R. Weiss, M. Rossi, J. Hu, K. Hu, K. Eitel, P. Gmeiner, J. Wess, B. K. Kobilka, B.K. Shoichet, Muscarinic receptors as model targets and antitargets for structure-based ligand discovery, Mol. Pharmacol. 84 (2013) 528–540, https://doi.org/10.1124/mol.113.087551.

[43] D.R. Weiss, J. Karpiak, X.P. Huang, M.F. Sassano, J. Lyu, B.L. Roth, B.K. Shoichet, Selectivity challenges in docking screens for GPCR targets and antitargets, J. Med. Chem. 61 (2018) 6830–6845, https://doi.org/10.1021/acs.jmedchem.8b00718.

[44] X. Barril, X. Fradera, Incorporating protein flexibility into docking and structure-based drug design, Exp. Opin. Drug Discov. 1 (2006) 335–349, https://doi.org/10.1517/17460441.1.4.335.

[45] P. Matricon, A. Ranganathan, E. Warnick, Z.G. Gao, A. Rudling, C. Lambertucci, G. Marucci, A. Ezzati, M. Jaiteh, D. Dal Ben, K.A. Jacobson, J. Carlsson, Fragment optimization for GPCRs by molecular dynamics free energy calculations: probing druggable subpockets of the A_{2A} adenosine receptor binding site, Sci. Rep. 7 (2017) 6398, https://doi.org/10.1038/s41598-017-04905-0.

[46] P. Matricon, R.R. Suresh, Z.G. Gao, N. Panel, K.A. Jacobson, J. Carlsson, Ligand design by targeting a binding site water, Chem. Sci. 12 (2021) 960–968, https://doi.org/10.1039/d0sc04938g.

[47] F. Deflorian, L. Pérez-Benito, E.B. Lenselink, M. Congreve, H. Van Vlijmen, J. S. Mason, C. de Graaf, G. Tresadern, Accurate prediction of GPCR ligand binding affinity with free energy perturbation, J. Chem. Inf. Model. 60 (2020) 5563–5579, https://doi.org/10.1021/acs.jcim.0c00449.

[48] W. Jespers, A. Oliveira, R. Prieto-Díaz, M. Majellaro, J. Åqvist, E. Sotelo, H. Gutiérrez-De-Terán, Structure-based design of potent and selective ligands at the four adenosine receptors, Molecules 22 (2017) 1945, https://doi.org/10.3390/molecules22111945.

[49] G. Mattedi, F. Deflorian, J.S. Mason, C. De Graaf, F.L. Gervasio, Understanding ligand binding selectivity in a prototypical GPCR family, J. Chem. Inf. Model. 59 (2019) 2830–2836, https://doi.org/10.1021/acs.jcim.9b00298.

[50] G. Bolcato, M. Bissaro, G. Deganutti, M. Sturlese, S. Moro, New insights into key determinants for adenosine 1 receptor antagonists selectivity using supervised molecular dynamics simulations, Biomolecules 10 (2020) 732, https://doi.org/10.3390/biom10050732.

[51] P. Matricon, D.D. Vo, Z.G. Gao, J. Kihlberg, K.A. Jacobson, J. Carlsson, Fragment-based design of selective GPCR ligands guided by free energy simulations, Chem. Commun. 57 (2021) 12305–12308, https://doi.org/10.1039/d1cc03202j.

[52] D. Lorber, B. Shoichet, Hierarchical docking of databases of multiple ligand conformations, Curr. Top. Med. Chem. 5 (2005) 739–749, https://doi.org/10.2174/1568026054637683.

[53] W. Liu, E. Chun, A.A. Thompson, P. Chubukov, F. Xu, V. Katritch, G.W. Han, C. B. Roth, L.H. Heitman, A.P. Ijzerman, V. Cherezov, R.C. Stevens, Structural basis for allosteric regulation of GPCRS by sodium ions, Science 337 (2012) 232–236, https://doi.org/10.1126/science.1219218.

[54] T. Hino, T. Arakawa, H. Iwanari, T. Yurugi-Kobayashi, C. Ikeda-Suno, Y. Nakada-Nakura, O. Kusano-Arai, S. Weyand, T. Shimamura, N. Nomura, A.D. Cameron, T. Kobayashi, T. Hamakubo, S. Iwata, T. Murata, G-protein-coupled receptor inactivation by an allosteric inverse-agonist antibody, Nature 482 (2012) 237–240, https://doi.org/10.1038/nature10750.

[55] A.S. Doré, N. Robertson, J.C. Errey, I. Ng, K. Hollenstein, B. Tehan, E. Hurrell, K. Bennett, M. Congreve, F. Magnani, C.G. Tate, M. Weir, F.H. Marshall, Structure of the adenosine A_{2A} receptor in complex with ZM241385 and the xanthines XAC and caffeine, Structure 19 (2011) 1283–1293, https://doi.org/10.1016/j.str.2011.06.014.

[56] G. Lebon, T. Warne, P.C. Edwards, K. Bennett, C.J. Langmead, A.G.W. Leslie, C. G. Tate, Agonist-bound adenosine A_{2A} receptor structures reveal common features of GPCR activation, Nature 474 (2011) 521–525, https://doi.org/10.1038/nature10136.

[57] G. Lebon, P.C. Edwards, A.G.W. Leslie, C.G. Tate, Molecular determinants of CGS21680 binding to the human adenosine A_{2A} receptor, Mol. Pharmacol. 87 (2015) 907–915, https://doi.org/10.1124/mol.114.097360.

[58] B. Carpenter, R. Nehmé, T. Warne, A.G.W. Leslie, C.G. Tate, Structure of the adenosine A_{2A} receptor bound to an engineered G protein, Nature 536 (2016) 104–107, https://doi.org/10.1038/nature18966.

[59] J.J. Irwin, T. Sterling, M.M. Mysinger, E.S. Bolstad, R.G. Coleman, ZINC: a free tool to discover chemistry for biology, J. Chem. Inf. Model. 52 (2012) 1757–1768, https://doi.org/10.1021/ci3001277.

[60] B.I. Tingle, K.G. Tang, M. Castanon, J.J. Gutierrez, M. Khurelbaatar, C. Dandarchuluun, Y.S. Moroz, J.J. Irwin, ZINC-22—A free multi-billion-scale database of tangible compounds for ligand discovery, J. Chem. Inf. Model. 63 (2023) 1166–1176, https://doi.org/10.1021/acs.jcim.2c01253.

[61] M. Jörg, A. Glukhova, A. Abdul-Ridha, E.A. Vecchio, A.T.N. Nguyen, P.M. Sexton, P.J. White, L.T. May, A. Christopoulos, P.J. Scammells, Novel irreversible agonists acting at the A_1 adenosine receptor, J. Med. Chem. 59 (2016) 11182–11194, https://doi.org/10.1021/acs.jmedchem.6b01561.

[62] A.T.N. Nguyen, J.A. Baltos, T. Thomas, T.D. Nguyen, L.L. Muñoz, K.J. Gregory, P. J. White, P.M. Sexton, A. Christopoulos, L.T. May, Extracellular loop 2 of the adenosine A_1 receptor has a key role in orthosteric ligand affinity and agonist efficacy, Mol. Pharmacol. 90 (2016) 703–714, https://doi.org/10.1124/mol.116.105007.

[63] S. Lazareno, N.J.M. Birdsall, Estimation of competitive antagonist affinity from functional inhibition curves using the Gaddum, Schild and Cheng-Prusoff equations, Br. J. Pharmacol. 109 (1993) 1110–1119, https://doi.org/10.1111/j.1476-5381.1993.tb13737.x.